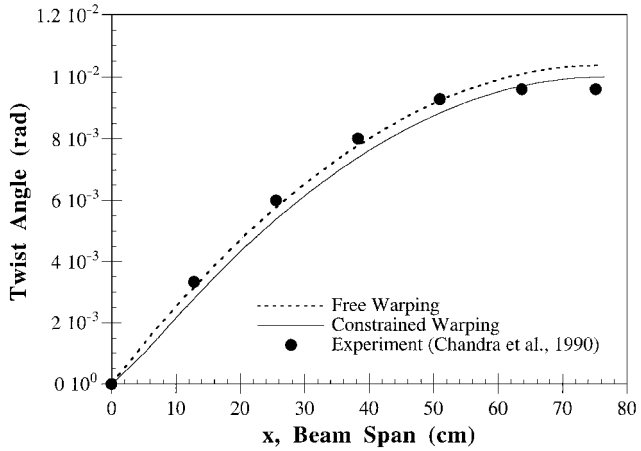

Fig. 2 Bending-induced twist angle of CAS1 beam A acted upon by 4.45-N tip shear load.

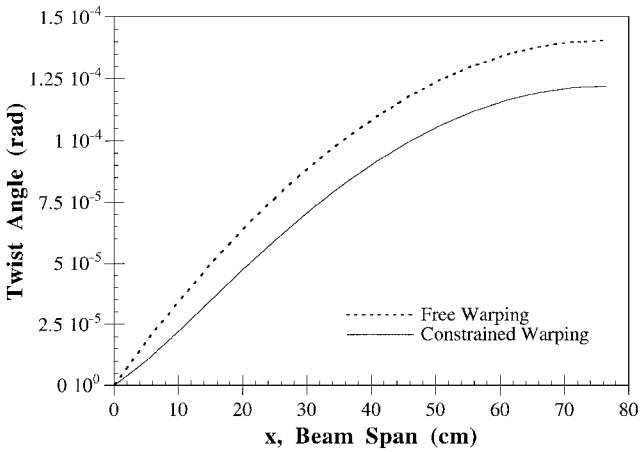

Fig. 3 Bending-induced twist angle of CAS1 beam B acted upon by 4.45-N tip shear load.

sequences, induced deformations, and slenderness ratio. Neglecting this effect by using a St. Venant torsional analysis can give erroneous results and significant underprediction of stresses in some cases.

Conclusions

The constrained warping effect is found to be significant enough to be included in the analysis of composite hollow beams in certain circumstances. A small nondimensional warping decay parameter (λL) gives a large critical length of constrained warping (x_{cr}). This length depends on the geometry and the mechanical properties of the beam. Larger x_{cr} of composite hollow beams compared to isotropic hollow beams indicates that constrained warping in composites is of more significance. A large slenderness ratio tends to mitigate the effects of constrained warping. In one of the examples (slenderness ratio = 8, $\lambda L = 25$), the bending-induced twist angle was shown to be reduced by 13% because of the constraint effect. Additional stresses caused by constrained warping can be very high. An example shows that maximum N_{xs} and N_{xx} at the support are higher by 26 and 143% than free warping.

References

[1]Chandra, R., Stemple, A. D., and Chopra, I., "Thin-Walled Composite Beams Under Bending, Torsional, and Extensional Loads," *Journal of Aircraft*, Vol. 27, No. 7, 1990, pp. 619–626.

[2]Berdichevsky, V., Armanios, E., and Badir, A., "Theory of Anisotropic Thin-Walled Closed-Cross-Section Beams," *Composite Engineering*, Vol. 2, Nos. 5–7, 1992, pp. 411–432.

[3]Rehfield, L. W., Atilgan, A. R., and Hodges, D. H., "Nonclassical Behavior of Thin-Walled Composite Beams with Closed Cross Sections," *Journal of the American Helicopter Society*, Vol. 35, No. 2, 1990, pp. 42–50.

[4]Kim, C., and White, S. R., "Analysis of Thick Hollow Composite Beams Under General Loadings," *Composite Structures*, Vol. 34, 1996, pp. 263–277.

[5]Vasiliev, V. V., *Mechanics of Composite Structures*, Taylor and Francis, Washington, DC, 1993.

[6]Benscoter, S. U., "A Theory of Torsion Bending for Multicell Beams," *Journal of Applied Mechanics*, Vol. 21, No. 1, 1954, pp. 25–34.

R. K. Kapania
Associate Editor

Convergence of Methods for Nonlinear Eigenvalue Problems

Per Bäck* and Ulf Ringertz†
Royal Institute of Technology, S-100 44 Stockholm, Sweden

Nomenclature

$\boldsymbol{A}$ = matrix of aerodynamic forces
b = semichord
$\boldsymbol{K}$ = stiffness matrix
k = reduced frequency, $\omega b/u$
M = Mach number
$\boldsymbol{M}$ = consistent mass matrix
p = eigenvalue
q = dynamic pressure, $\rho u^2/2$
$\hat{q}$ = nondimensional dynamic pressure; $\hat{q} \in (0, 1)$
u = airspeed
$\tilde{\boldsymbol{v}}$ = eigenvector
ρ = air density
$\boldsymbol{\Omega}$ = diagonal matrix with free vibration frequencies
ω = vibration frequency

Introduction

ALTHOUGH significant advances have been made in the use of nonlinear fluid mechanics models for aeroelasticity analysis,[1] most analysis is still performed using linear unsteady potential flow models. Combining linear elastic structural dynamics with linear unsteady potential flow, it is possible to analyze the stability of quite complex aircraft structures by solving a nonlinear eigenvalue problem. There are several different methods available for the solution of nonlinear eigenvalue problems,[2] and this Note focuses on the convergence properties of a particular method known as the p–k method.

Assuming linear structural dynamics, the equations of motion for an aircraft wing structure may be given in discretized form as

$$\boldsymbol{M}\ddot{\boldsymbol{v}} + \boldsymbol{K}\boldsymbol{v} = \boldsymbol{f}(t) \tag{1}$$

where the vector $\boldsymbol{v} \in R^n$ denotes the nodal displacements of the wing finite element model.

Assuming linear unsteady aerodynamics and transforming the equations to the frequency domain gives the eigenvalue problem

$$[p^2\boldsymbol{M} + \boldsymbol{K} - q\boldsymbol{A}(M, p)]\tilde{\boldsymbol{v}} = 0 \tag{2}$$

Following standard procedures,[2] the eigenvalue problem is transformed using a modal subspace into the nondimensional form given by

$$[\hat{p}^2\boldsymbol{I} + \boldsymbol{\Omega}^2 - \hat{q}\hat{\boldsymbol{A}}(\hat{p}, M)]\hat{\boldsymbol{v}} = 0 \tag{3}$$

where $\hat{\boldsymbol{v}} \in R^m$ and usually with $m \ll n$. The nondimensional eigenvalue $\hat{p}$ is defined such that the imaginary part equals the reduced frequency k.

Received June 25, 1996; revision received Jan. 31, 1997; accepted for publication March 17, 1997.

*Graduate Student, Department of Aeronautics.
†Associate Professor, Department of Aeronautics. Member AIAA.

The significant difficulty with the eigenvalue problem (3) is that the complex matrix of aerodynamic forces depends on both the eigenvalue $\hat{p}$ and the Mach number M.

p–k Method

Perhaps the most popular method for solving the nonlinear eigenvalue problem is the so-called *p–k* method. In this case, the aerodynamic forces are only computed for purely imaginary values of $\hat{p}$ giving the nonlinear eigenvalue problem

$$[\hat{q}\hat{\boldsymbol{A}}(\mathrm{Im}\,\hat{p}, M) - \boldsymbol{\Omega}^2 - \hat{p}^2\boldsymbol{I}]\hat{\boldsymbol{v}} = 0 \tag{4}$$

The nonlinear eigenvalue problem is solved for given values of $\hat{q}$ and M representing a flight condition. The system is stable for the flight condition if all the eigenvalues $\hat{p}$ have negative real part.

The eigenvalues are traced from vacuum ($\hat{q} = 0$), where the eigenvalues are known, using $\hat{q}$ as a continuation parameter for each flight condition. For each value of $\hat{q}$, the aerodynamic forces are computed for the current approximation of the reduced frequency $k = \mathrm{Im}\,\hat{p}^l$, and the new approximation to the eigenvalue is obtained by solving

$$[\hat{q}\hat{\boldsymbol{A}}(k, M) - \boldsymbol{\Omega}^2 - (\hat{p}^{l+1})^2\boldsymbol{I}]\hat{\boldsymbol{v}} = 0 \tag{5}$$

The reduced frequency is then set to the new value $k = \mathrm{Im}\,\hat{p}^{l+1}$ and the process repeated for each eigenvalue until convergence.

This simple method has repeatedly been demonstrated to be useful and appears to be the most used method in the aircraft industry today. However, the method is not without problems.

The first and perhaps most obvious deficiency of the *p–k* method is that convergence is sometimes very slow. It is usually sufficient with approximately 10 iterations to obtain a relative accuracy in $\hat{p}_i$ of 10^{-7}. However, in some cases, even several hundred iterations are not enough to reach this accuracy. Apparently, it would be highly desirable to characterize what slows convergence and perhaps improve the robustness of the method.

A second difficulty is that it may not be possible to trace all the eigenvalues as functions of $\hat{q}$. The radius of convergence for the *p–k* method may be very close to zero, meaning that very small increments in $\hat{q}$ may be required to trace all the individual eigenvalues. To illustrate this difficulty, consider the root-locus plot shown in Fig. 1.

The root-locus plot was obtained by solving the nonlinear eigenvalue problem using the basic *p–k* method with a very small increment in $\hat{q}$ of $\delta_{\hat{q}} = 10^{-3}$. The structure represents a cantilever rectangular wing modeled as a full depth sandwich structure using Mindlin plate finite elements for the structure and the doublet lattice scheme of Albano and Rodden[3] for the aerodynamic forces. A detailed description of the test case is given in Ref. 4.

The initial eigenvalues for $\hat{q} = 0$ are shown with the $\times$ symbol, and the eigenvalues are then shown as dots for increasing $\hat{q}$. The eigenvalues are numbered so that the eigenvalue with the smallest imaginary part comes first for $\hat{q} = 0$. It is clear from Fig. 1 that eigenvalues $\hat{p}_3$ and $\hat{p}_4$ become very close for a particular value of $\hat{q}$. For the next increment in $\hat{q}$ the *p–k* method cannot distinguish the two eigenvalues, and the algorithm converges to the same value despite slightly different initial values for $\hat{p}_3$ and $\hat{p}_4$.

Modifications to the Basic Algorithm

The basic *p–k* algorithm can be seen as applying a method for univariate zero finding to the nonlinear equation

$$\mathrm{Im}\,\hat{p}(k) - k = 0 \tag{6}$$

where $\hat{p}(k)$ denotes an eigenvalue obtained by solving the linear eigenvalue problem

$$[\hat{q}\hat{\boldsymbol{A}}(k, M) - \boldsymbol{\Omega}^2 - \hat{p}^2\boldsymbol{I}]\hat{\boldsymbol{v}} = 0 \tag{7}$$

for a given value of the reduced frequency k and a fixed flight condition.

Applying direct iteration to the nonlinear equation gives the algorithm

$$k^{l+1} = \mathrm{Im}\,\hat{p}(k^l) \tag{8}$$

which is known to converge locally,[5] provided that the condition

$$\left|\mathrm{Im}\frac{\mathrm{d}\hat{p}}{\mathrm{d}k}(k*)\right| < 1 \tag{9}$$

holds, where $k*$ denotes a solution to Eq. (6). Unfortunately, the asymptotic convergence rate is only linear, meaning that

$$\lim_{l\to\infty}\frac{|\hat{p}^{l+1} - \hat{p}*|}{|\hat{p}^l - \hat{p}*|} = \left|\mathrm{Im}\frac{\mathrm{d}\hat{p}}{\mathrm{d}k}(k*)\right| < 1 \tag{10}$$

Further, the basic algorithm does not converge if the derivative is greater than one in magnitude, and convergence is extremely slow if the derivative is close to one.

To illustrate that the derivative of $\hat{p}$ with respect to k can indeed be greater than one, consider the graph shown in Fig. 2. The eigenvalues Im p are shown as functions of the reduced frequency for the wing described in the preceding section and a flight condition with $M = 0.7$ and $\hat{q} = 1$. As expected, the basic *p–k* algorithm converges extremely slowly on the two smallest eigenvalues even if a good initial approximation is provided.

However, it is possible to significantly improve the convergence rate by using Newton's methods for solving the nonlinear equation (6). Applying Newton's method to Eq. (6) gives the algorithm

$$k^{l+1} = k^l - \frac{\mathrm{Im}\,\hat{p}(k^l) - k^l}{\mathrm{Im}\,(\mathrm{d}\hat{p}/\mathrm{d}k)(k^l) - 1} \tag{11}$$

which converges to $p*$ if the initial approximation is sufficiently close. The important difference is that the asymptotic convergence rate is quadratic, meaning

$$\lim_{l\to\infty}\frac{|\hat{p}^{l+1} - \hat{p}*|}{|\hat{p}^l - \hat{p}*|^2} = \beta \tag{12}$$

where β is some constant.

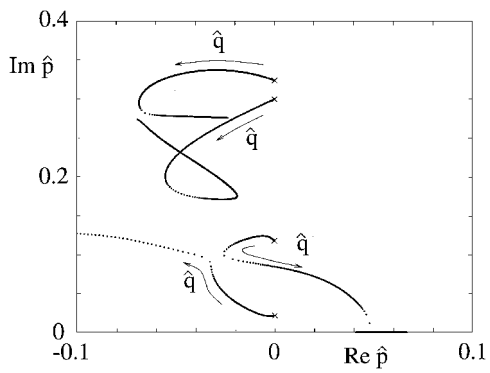

Fig. 1 Root-locus plot obtained using the basic *p–k* method: $M = 0.8$.

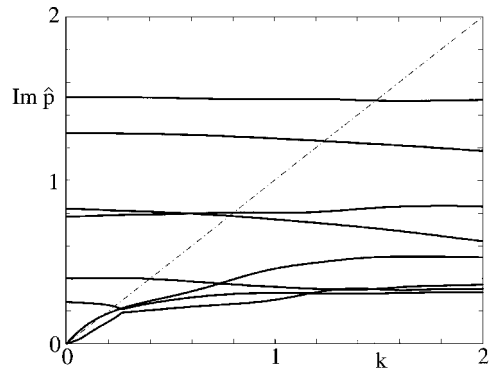

Fig. 2 Imaginary part of the eigenvalues as functions of *k*: $M = 0.7$.

Unfortunately, the basic Newton algorithm is not globally convergent and needs to be combined with some safeguards to guarantee convergence from poor initial approximations. The safeguards are also needed to take care of the case when the derivative $\mathrm{Im}(\mathrm{d}\hat{p}/\mathrm{d}k)(k^j)$ is 1 or close to 1. The implementation of a safeguarded Newton method is relatively straightforward; see Ref. 5 for further details.

The improvement obtained using Newton's method compared with the basic p–k algorithm is dramatic. Only 5–10 iterations are needed to obtain full machine precision for cases where the p–k algorithm requires hundreds of iterations to obtain only modest accuracy.

The derivative of the square of the eigenvalue is given by

$$\frac{\mathrm{d}\hat{p}^2}{\mathrm{d}k} = \hat{\boldsymbol{v}}_L^H \left[\hat{q} \frac{\mathrm{d}}{\mathrm{d}k} \hat{\boldsymbol{A}}(k, M) \right] \hat{\boldsymbol{v}}_R \Big/ \hat{\boldsymbol{v}}_L^H \hat{\boldsymbol{v}}_R \tag{13}$$

where $\hat{\boldsymbol{v}}_L^H$ denotes the Hermitian transpose of the left eigenvector and $\hat{\boldsymbol{v}}_R$ denotes the right eigenvector to Eq. (7). The derivative of the eigenvalue itself is simply given by

$$\frac{\mathrm{d}\hat{p}}{\mathrm{d}k} = \frac{\mathrm{d}\hat{p}^2}{\mathrm{d}k} \Big/ (2\hat{p}) \tag{14}$$

The derivative of the eigenvalue requires only a modest additional computation because the derivative of the matrix $\boldsymbol{A}(k, M)$ is easy to obtain by differentiating the spline functions used to interpolate the aerodynamic forces for arbitrary values of k.

It is also apparent from Fig. 2 that the number of solutions to the nonlinear equation (6) may be more than the dimension m of the eigenvalue problem. The number of eigenvalues to Eq. (7) for a given reduced frequency is always m, including possible multiplicities. However, a single eigenmode may cross the line $\mathrm{Im}\,\hat{p}(k) = k$ more than 1 time.

Figure 2 illustrates this case clearly. For $k = 0$, two modes have $\mathrm{Im}\,\hat{p} = 0$. But one of these two modes crosses the line $\mathrm{Im}\,\hat{p}(k) = k$ again for $k \approx 0.16$. Consequently, there are in this particular case nine distinct roots to the nonlinear eigenvalue problem (4) with $m = 8$.

The standard p–k procedure involves tracing the eigenvalues from vacuum using the dynamic pressure as parameter. Unfortunately, this implies that only m eigenvalues can be traced, meaning that important roots to the nonlinear eigenvalue problem may be missed.

A much better approach is to follow the eigenvalues $\hat{p}$ as functions of the reduced frequency for a fixed flight condition and dynamic pressure. The number of eigenvalues for each value of k is known, and the task is to establish the number of times the line $\mathrm{Im}\,\hat{p}(k) = k$ is crossed.

The first step of the algorithm is to establish lower $\underline{k}$ and upper $\bar{k}$ bounds for the imaginary part of each eigenvalue that is a root to the nonlinear eigenvalue problem (4). The eigenvalues to the linear eigenvalue problem (7) are first found for $k = 0$. The number of eigenvalues with $\mathrm{Im}\,\hat{p}(0) = 0$ are stored as roots to Eq. (4). Such eigenvalues come in pairs with real part $\pm\hat{p}(0)$. There are two such eigenvalue pairs for the case shown in Fig. 2.

The derivative equation (14) is then computed for $k = 0$ and used to establish whether any of the eigenvalues with $\mathrm{Im}\,\hat{p}(0) = 0$ will cross the line $\mathrm{Im}\,\hat{p}(k) = k$ for $k > 0$. If the derivative is greater than 1, the eigenvalue will cross the line for $k > 0$. In Fig. 2, one eigenvalue has a derivative greater than 1 and the other has a derivative less than 1. Consequently, there will be at least $m + 1$ roots to the nonlinear eigenvalue problem (4).

The algorithm for establishing the lower $\underline{k}$ and upper $\bar{k}$ bounds is essentially bisection. An initial step $k = \Delta k$ is taken, the eigenvalues $\hat{p}(k)$ are computed and sorted with respect to imaginary part, and the number of modes crossing the line $\mathrm{Im}\,\hat{p}(k) = k$ is established. If the number of crossings n_c is zero, a new step $k = k + \Delta k$ is taken. If $n_c = 1$, upper and lower bounds have been found. Finally, if $n_c > 1$, the step is reduced as $\Delta k = \Delta k/2$. The process is repeated until the lower and upper bounds have been found for k in the range $[0, k_{\max}]$.

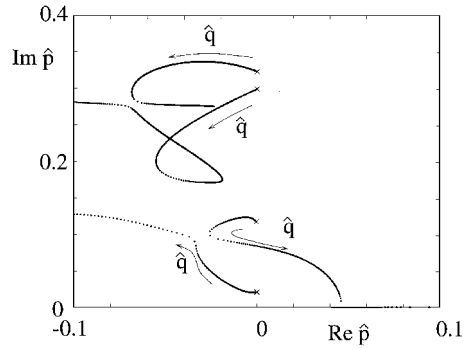

Fig. 3 Root-locus plot obtained using the modified method: $M = 0.8$.

The value for Δk is somewhat arbitrary; it will be reduced if too large and increased if too small. If the eigenvalue $\hat{p}(0)$ has zero imaginary parts and the derivative satisfies $\mathrm{Im}(\mathrm{d}\hat{p}_i/\mathrm{d}k)(0) < 1$, then the eigenvalue $\hat{p}_i(0)$ is set to a small negative value $-\epsilon$ to ensure that the number of crossings of the line $\mathrm{Im}\,\hat{p}(k) = k$ is correctly computed.

The use of the algorithm ensures that the number of roots n_r is correctly computed as well as establishes upper and lower bounds for each of the roots with $\mathrm{Im}\,\hat{p} > 0$. These bounds can now be used in a safeguarded Newton method for accurate determination of all the desired eigenvalues.

The safeguarded Newton method tries to take the pure Newton step on each iteration if at least a moderate reduction is obtained in the residual. If the reduction is not sufficient, the method switches to bisection. This way the local quadratic convergence rate of Newton's method is combined with the robustness of bisection. If there are two modes that cross the line $\mathrm{Im}\,\hat{p}(k) = k$ for the same value of k, the rate of convergence is reduced to that of bisection. Consequently, bisection is also used if there are coalescing eigenvalues to Eq. (7) for which the derivative equation (13) does not exist.

It is now interesting to present results obtained using the modified method in a root-locus plot similar to Fig. 1, where the basic p–k method was used. The root-locus plot in Fig. 3 shows the eigenvalues computed using the modified method for the same dynamic pressures considered in Fig. 1. The improvement obtained using the modified method is obvious if Figs. 1 and 3 are compared. The modified method easily establishes the correct number and location of all the eigenvalues of the nonlinear eigenvalue problem (4), whereas the basic p–k method fails despite the very small steps taken in $\hat{q}$.

Conclusion

The modified method is not more efficient than the basic p–k algorithm if the eigenvalues are easy to find, for example, when the derivative $\mathrm{Im}(\mathrm{d}\hat{p}/\mathrm{d}k)$ is close to 0. However, for the more difficult cases where small steps in dynamic pressure are necessary or convergence of the basic algorithm is slow, the modified method may be many orders of magnitude more efficient. Note that it is not necessary to trace the eigenvalues, with the dynamic pressure as a parameter, to find the eigenvalues for a particular flight condition if the modified method is used.

Acknowledgments

Per Bäck was supported by the National Program for Aeronautics Research. Ulf Ringertz was supported by the Swedish Research Council for Engineering Sciences.

References

[1]Obayashi, S., Guruswamy, G. P., and Goorjian, P. M., "Streamwise Upwind Algorithm for Computing Unsteady Transonic Flows Past Oscillating Wings," *AIAA Journal*, Vol. 29, No. 10, 1991, pp. 1668–1677.

[2]Dowell, E. H., Curtiss, H. C., Scanlan, R. H., and Sisto, F., *A Modern Course in Aeroelasticity*, Kluwer, Dordrecht, The Netherlands, 1989.

[3]Albano, E., and Rodden, W. P., "A Doublet-Lattice Method for Calculating Lift Distributions on Oscillating Surfaces in Subsonic Flows," *AIAA Journal*, Vol. 7, No. 2, 1969, pp. 279–285.

[4]Ringertz, U. T., "On Structural Optimization with Aeroelasticity Constraints," *Structural Optimization*, Vol. 8, No. 1, 1994, pp. 16–23.

[5]Gill, P. E., Murray, W., and Wright, M. H., *Practical Optimization*, Academic, London, 1981.

R. K. Kapania
Associate Editor

Reduced-Order Aeroservoelastic Model with an Unsteady Aerodynamic Eigen Formulation

Taehyoun Kim*
Georgia Institute of Technology, Atlanta, Georgia 30332
Changho Nam†
Hankuk Aviation University, Koyang 411-791, Korea
and
Youdan Kim‡
Seoul National University, Seoul 151-742, Korea

Introduction

A DIFFICULTY in using modern control theory for the design of aeroelastic control systems is the requirement of transforming the unsteady aerodynamic forces, normally provided in the frequency domain, into the time domain. The usual procedure is to approximate the unsteady aerodynamic force as a rational function in the Laplace domain.

Recently, a new formulation called eigenanalysis of unsteady aerodynamics has provided a direct representation of the unsteady aerodynamic loads in the time domain.[1] The eigenmethods suggested so far rely on the discrete-time domain formulation that may result in reduced-order models with complex coefficients. For the designs of closed-loop aeroelastic systems, however, it is preferable to have aerodynamic models with real coefficients in the continuous-time domain. The purpose of this study is to construct a new aeroservoelastic model using a two-dimensional, incompressible aerodynamic eigenformulation in the continuous-time domain. The work is based on the discrete-time domain eigen model by Hall.[2] To obtain a reduced-order model with real coefficients, a modal decomposition technique that transforms the aerodynamic matrix into a canonical modal form is introduced. A simple typical section model with two strain-actuated control inputs is used for an aeroservoelastic design.

Unsteady Aerodynamic Modeling

We divide the bound vortex representing the airfoil into M elements and divide the free vortex representing the traveling wake into $(N - M)$ elements. The total number of vortex elements is N.

Given an $(M \times 1)$ bound vortex vector $\boldsymbol{\Gamma}_1$ and an $[(N - M) \times 1]$ wake vortex vector $\boldsymbol{\Gamma}_2$, the downwash in the discrete-space domain is expressed as

$$\boldsymbol{W}_{\frac{3}{4}} = [\boldsymbol{K}_1 \quad \boldsymbol{K}_2] \begin{Bmatrix} \boldsymbol{\Gamma}_1 \\ \boldsymbol{\Gamma}_2 \end{Bmatrix} \tag{1}$$

where $\boldsymbol{W}_{3/4}$ is an $(M \times 1)$ vector containing downwashes at three-quarter points of the airfoil elements and $\boldsymbol{K}_1$ and $\boldsymbol{K}_2$ are the two-dimensional kernel function matrices.

For conservation of vorticity in the discrete-space domain, it is required that

$$-\boldsymbol{S}_1 \dot{\boldsymbol{\Gamma}}_1 = (\Gamma_{M+1}/\Delta x)U \tag{2}$$

with $\boldsymbol{S}_1 \equiv [1 \quad 1 \quad \cdots \quad 1]_{(1 \times M)}$. For the special case of $\Delta x = U\Delta t$, we can write

$$\Gamma^{n+1}_{M+1} + \Gamma^{n}_{M+1} = -2 \sum_{i}^{M} (\Gamma^{n+1}_{i} - \Gamma^{n}_{i}) \tag{3}$$

For convection of free wakes, we have

$$\dot{\Gamma}_i = -U \frac{\partial \Gamma_i}{\partial x} \qquad (i = M+2, \ldots, N) \tag{4}$$

The free wake convection is conveniently described in the discrete-time domain as

$$\begin{aligned} \Gamma^{n+1}_{i} &= \Gamma^{n}_{i-1} \qquad (i = M+2, \ldots, N-1) \\ \Gamma^{n+1}_{N} &= w\Gamma^{n}_{N} + \Gamma^{n}_{N-1} \qquad (0.95 < w < 1) \end{aligned} \tag{5}$$

The weighting factor w in Eq. (5) is introduced to prevent sudden change in the induced downwash due to the finite length of the wake vortex sheet.[2]

By putting Eqs. (1), (2), and (4) together, one can write the continuous model in matrix form:

$$\boldsymbol{A}_a \dot{\boldsymbol{\Gamma}}_2 = (U/\Delta x)\boldsymbol{B}_a \boldsymbol{\Gamma}_2 + \boldsymbol{C}_a \dot{\boldsymbol{W}}_{\frac{3}{4}} \tag{6}$$

The corresponding discrete model can be written in a fashion similar to but simpler than that of Hall[2] as

$$\boldsymbol{A}_{ad} \boldsymbol{\Gamma}^{n+1}_{2} = \boldsymbol{B}_{ad} \boldsymbol{\Gamma}^{n}_{2} + \boldsymbol{C}_{ad} \dot{\boldsymbol{W}}^{n+1}_{\frac{3}{4}} \tag{7}$$

where the time step in this discrete model is $\Delta t = \Delta x/U$. In the preceding equations, all matrices are known except for $\boldsymbol{B}_a$. It can be obtained by integrating Eq. (6) from $t = t^n$ to $t = t^{n+1}$ and comparing the homogeneous part with that of Eq. (7):

$$\boldsymbol{B}_a = \boldsymbol{A}_a \ln(\boldsymbol{A}^{-1}_{ad} \boldsymbol{B}_{ad}) \tag{8}$$

Reduced-Order Aeroservoelastic Model

To obtain a reduced-order model with real coefficients, we first transform the aerodynamic matrix into a canonical modal form,

$$\boldsymbol{A}_{\text{can}} = \boldsymbol{Q}^T (\boldsymbol{A}^{-1}_{a} \boldsymbol{B}_a) \boldsymbol{P}, \qquad \boldsymbol{Q}^T \boldsymbol{P} = \boldsymbol{I}_{N-M} \tag{9}$$

where $\boldsymbol{P}$ and $\boldsymbol{Q}^T$, respectively, contain the right and left eigenvectors of the system. In this form, pairs of complex conjugate eigenvalues appear in (2×2) blocks along the diagonal, and the real eigenvalues appear on the diagonal. We next decompose the unsteady vortex into

$$\bar{\boldsymbol{\Gamma}}_2 \simeq \boldsymbol{P}_R \boldsymbol{q} + \bar{\boldsymbol{\Gamma}}_s \tag{10}$$

where $\boldsymbol{P}_R$ contains the N_R columns of $\boldsymbol{P}$ corresponding to the selected N_R eigenvalues, $\boldsymbol{q}$ is the generalized coordinate vector, and $\bar{\boldsymbol{\Gamma}}_s$ is a static correction.

Finally, for a typical section undergoing plunging $\bar{h}$ and pitching motion α with bending and torsion strain actuation u_h and u_α, respectively, one can write nondimensional aeroservoelastic equations of motion in the following form:

$$\boldsymbol{A}\dot{\boldsymbol{X}} = \boldsymbol{B}\boldsymbol{X} + \boldsymbol{C}\boldsymbol{u} \tag{11}$$

Received Aug. 16, 1995; revision received Jan. 3, 1997; accepted for publication March 17, 1997.

*Research Scientist, Computational Mechanics Center; currently Senior Specialist Engineer, Boeing Commercial Airplane Group, P.O. Box 3707, MS 67-HM, Seattle, WA 98124. Member AIAA.

†Assistant Professor, Department of Aeronautical and Mechanical Engineering. Member AIAA.

‡Assistant Professor, Department of Aerospace Engineering. Member AIAA.